Journal of Thermal Analysis and Calorimetry (2020) 140:1801–1810
https://doi.org/10.1007/s10973-019-08918-x

Thermal decomposition behaviour and kinetics of a mixed solution: *n*-propyl nitrate and nitric acid solution

Qiang Xie[1] · Yong Xie[2] · Wei Liu[1] · Lei Zhang[1] · Shi Li[1] · Houhe Chen[1]

Received: 5 June 2019 / Accepted: 12 October 2019 / Published online: 2 November 2019
© Akadémiai Kiadó, Budapest, Hungary 2019

Abstract
To provide a theoretical basis for improving the thermal safety of spent acid, its decomposition behaviour was studied. A mixed solution of *n*-propyl nitrate (NPN) and nitric acid was analysed using isoperibolic experiments and differential scanning calorimetry. An accurate kinetic model based on the analysis was proposed to describe the decomposition of the spent acid by applying an isoconversional method and nonlinear regression to the DSC data. We found that the thermal decomposition in the mixed solution involved two competing reactions: the decomposition of NPN in the nitric acid solution and the decomposition of nitric acid. The decomposition of the mixed solution followed a 0.9082th Prout–Tompkins equation with autocatalysis, with a differential kinetic mechanism function of $f(\alpha)=(1-\alpha)^{0.9082}\cdot\alpha^{0.1291}$. Lastly, the thermal safety evaluation and thermodynamic parameters were studied. The self-accelerating decomposition temperature and the critical temperature of thermal runway were 338.70 K and 346.76 K, respectively, in an approximately closed system, and 347.25 K and 355.73 K, respectively, in an open system. These results show that the spent acid was more hazardous than the NPN and nitric acid solution. In addition, the thermal stability of the mixed solution in an open system was higher than that of the mixed solution in an approximately closed system.

Keywords Spent acid · Nitrate ester · Decomposition kinetics · Mechanism function · Self-accelerating decomposition temperature

Introduction

N-propyl nitrate (NPN, $C_3H_7O_3N$) is a nitrate ester by-product, that is, it is found in the residual acid solutions (spent acid) of industrial nitration processes. It is well known that spent acid sometimes undergoes violent decomposition reactions, which result in industrial accidents [1–3]. In addition, the large amounts of nitrogen dioxide produced by spent acid are harmful to humans and the environment [4].

Nitrate esters, as important liquid energetic materials, are widely used in mixed explosive and propellants. Therefore, several studies on the theoretical and experimental thermolysis of nitrate esters have been published [5–9]. Moreover, in recent years, some researchers have focused on nitrate esters in acid solutions to discuss the storage safety of nitrate esters. Camera et al. [10, 11] suggested that the nitrate esters in an acid solution containing sulphuric acid and a small amount of nitric acid were first hydrolysed into alcohols, which were then quickly oxidized into aldehydes and nitrous acid. Yang et al. [12] found that acid solutions (sulphuric acid solution, nitric acid solution, and mixed acid solution) could decrease the stability of 2-ethylhexyl nitrate (EHN) based on differential scanning calorimetry (DSC) and accelerating rate calorimetry (ARC) results. However, for the studies of these researchers, there is one thing in common: the nitrate ester content was not much smaller than that of the acid solution. In fact, the required content of the acid solution was large, and the yield of the by-products was small for the nitration process. Thus, there have been few reports on the thermal decomposition behaviour and kinetics of mixed solutions containing small amounts of nitrate ester and large nitric acid solution, which is similar to real spent acid from the nitration process.

Thermal analysis (TA) is a technology that can measure the relationship between the heat flow or mass of a sample

✉ Houhe Chen
chhh42792@sina.cn

[1] Chemical Engineering Institute, Nanjing University of Science and Technology, Nanjing, Jiangsu, China

[2] Hubei Dongfang Chemical Industry Company Limited, Norinco Group, Xiangyang, Hubei, China

and the temperature change. The TA results can also provide valuable parameters by using kinetic theory concerning the thermal decomposition of hazardous materials. For example, we can obtain most probable mechanism functions, the values of kinetic and thermodynamic parameters. Furthermore, TA results and these thermokinetic parameters, i.e. activation energy and frequency factor, can permit the prediction of thermal safety parameters including the critical ignition temperature [13–19]. Thus, TA techniques, such as DSC and thermogravimetry (TG), have widely been used to study the thermal decomposition, kinetics, and safety of hazardous materials due to these abilities.

In general, nitrolysis solution or other spent acids are unstable and hazardous and could cause industrial accidents, making them harmful to the environment. Therefore, the aim here is to study the decomposition characteristics, establish an accurate kinetic model to describe the pyrolysis of spent acid, and obtain thermodynamic parameters to estimate the thermal stability of a mixed solution, i.e. an NPN and nitric acid solution. We used isoperibolic experiments and non-isothermal DSC to study the decomposition behaviour and an isoconversional method and a nonlinear regression to establish a kinetic model and obtain the thermodynamic parameters.

Materials and methods

Materials

The mixed system used in this study was prepared from an NPN (2 mass%) and nitric acid solution (98 mass%). The NPN used was chemical grade. The nitric acid solution used was analytical grade, and its mass concentration was 65%.

Experimental

The isoperibolic experiments were performed on a homemade device that included a water bath, a test tube, a temperature sensor, and a paperless recorder, as shown in Fig. 1. Here, the temperature sensor was a Pt100 (Heraeus, Germany) with Teflon protection sleeve. The paperless recorder was made by Shanghai Yijie in China, and its accuracy was ±0.1 K. The mass of each sample was approximately 5 g, and various water bath temperatures were tested.

The DSC analysis was carried out on a previously calibrated DSC823e instrument (Mettler Toledo Co., Switzerland), and the DSC scans were performed at heating rates of 8, 10, and 12 K min^{-1}. For these measurements, approximately 15 mg of a sample was placed in an atmospheric pressure crucible (an aluminium pan with a small hole). The experiment was performed under a nitrogen atmosphere with a flow rate of 30 mL min^{-1} (purity 99.999%).

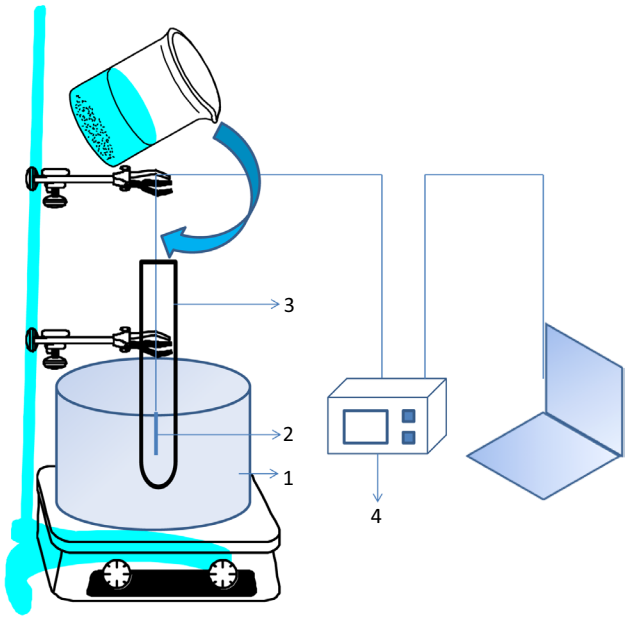

Fig. 1 Schematic diagram of the isoperibolic experimental set-up for thermal decomposition of NPN in nitric acid solution. (1) Water bath, (2) temperature sensor, (3) test tube, (4) paperless recorder

Kinetic analysis

According to the Arrhenius equation and the non-isothermal DSC data, the basic rate equation applied in this study can be expressed as:

$$\frac{\mathrm{d}\alpha}{\mathrm{d}T} = kf(\alpha) = \frac{A}{\beta}\exp\left(-\frac{E(\alpha)}{RT}\right)f(\alpha) \tag{1}$$

where α is the conversion degree, β is the heating rate /K min^{-1}, A is the pre-exponential factor /s^{-1}, $E(\alpha)$ is the activation energy /kJ mol^{-1}, T is the reaction temperature /K, $f(\alpha)$ is the differential kinetic mechanism function, and R is the gas constant (8.314 J mol^{-1} K^{-1}). The value α is given by Eqs. (2)–(3):

$$\alpha = \frac{H_0 - H_\mathrm{t}}{H_0 - H_\infty} \tag{2}$$

$$H_\mathrm{t} = \int_{t_0}^{\mathrm{t}} \frac{\mathrm{d}H}{\mathrm{d}t} \tag{3}$$

where H_0, H_t, and H_∞ represent the initial heat, the heat at time t, and the final heat, respectively.

Currently, there are various methods for determining the most probable mechanism function and kinetic parameters. Among these methods, the isoconversional method, which includes the Kissinger, Friedman, Kissinger–Akahira–Sunose (KAS), and Flynn–Wall–Ozawa (FWO) methods, is used to

determine the activation energy without having to choose a reaction mechanism function and is a classic and effective way to obtain the activation energy while avoiding imposing a reaction mechanism. Thus, in this paper, we first used the partial area integral to transform the DSC curves into curves of the conversion degree. Then, the Friedman and FWO methods were used to obtain the activation energy of decomposition. The most probable mechanism function was selected by nonlinear regression with the activation energy as a constant. Finally, model-free routes, i.e. the Kissinger and KAS methods, were used to check the calculated kinetic parameters.

The Friedman method [20, 21] considers the temperature dependence for a given degree of conversion as given by Eq. (4):

$$\ln\left(\beta\frac{\mathrm{d}\alpha}{\mathrm{d}T}\right) = \ln(Af(\alpha)) - \frac{E(\alpha)}{RT} \tag{4}$$

The FWO method [22, 23] was employed to calculate the kinetics and the function of the reciprocal temperature at any degree of conversion and is expressed in Eq. (5):

$$\lg\beta = \lg\left[\frac{A(\alpha)E(\alpha)}{RG(\alpha)}\right] - 2.315 - 0.4567\frac{E}{RT} \tag{5}$$

where $G(\alpha)$ is the integral kinetic mechanism function related to the differential kinetic mechanism function $f(\alpha)$ via Eq. (6):

$$G(\alpha) = \int_0^\alpha \frac{d\alpha}{f(\alpha)} \tag{6}$$

The Kissinger method [24, 25] is expressed by Eq. (7):

$$\ln\frac{\beta}{T_\mathrm{p}^2} = \ln\left[\frac{AE}{RG(\alpha_\mathrm{p})}\right] - \frac{E}{RT_\mathrm{p}} \tag{7}$$

where T_p is the peak temperature and α_p is the conversion degree at the peak temperature.

The KAS method [26, 27] is an extension of Kissinger method, as expressed by Eq. (8):

$$\ln\frac{\beta}{T^2} = \ln\left[\frac{AE}{RG(\alpha)}\right] - \frac{E}{RT} \tag{8}$$

An accurate kinetic model is important for investigating the decomposition in spent acid. In this study, the DSC data at different heating rates were fitted to typical reaction kinetic models collected from previous reports [28, 29] by nonlinear regression, as listed in Table 1. According to a study by Zhang et al. [30], the correlation coefficient was the primary criterion for selecting the most probable mechanism function for decomposition in a mixed solution. The least squares (LS) and mean residual (MR) values were used to determine the goodness of fit. These parameters are expressed by Eq. (9) and Eq. (10):

$$\mathrm{LS} = \mathrm{Min}\sum_{i=1}^{N}(\alpha_{\mathrm{exp,i}} - \alpha_{\mathrm{pre,i}})^2 \tag{9}$$

$$\mathrm{MR} = \frac{\sum_{i=1}^{N}\left|\alpha_{\mathrm{exp,i}} - \alpha_{\mathrm{pre,i}}\right|}{N} \tag{10}$$

Table 1 Typical reaction kinetic models used for nonlinear regression analysis

Model No.	Kinetic model	Abbreviation: $f(\alpha)$
1	Reaction first order	F1: $1-\alpha$
2	Reaction second order	F2: $(1-\alpha)^2$
3	Reaction of nth order	Fn: $(1-\alpha)^\mathrm{n}$
4	Phase boundary-controlled reaction (contracting cylinder)	R2: $(1-\alpha)^{1/2}$
5	Phase boundary-controlled reaction (contracting sphere)	R3: $(1-\alpha)^{2/3}$
6	Prout–Tompkins equation	B1: $\alpha(1-\alpha)$
7	*n*th Prout–Tompkins equation with autocatalysis	Bna: $(1-\alpha)^\mathrm{n}\cdot\alpha^\mathrm{a}$
8	Reaction of first order with autocatalysis	C1: $(1-\alpha)(1+\mathrm{J_{kat}}\,\alpha)$
9	Reaction of nth order with autocatalysis	C*n*: $(1-\alpha)^\mathrm{n}\cdot(1+\mathrm{J_{kat}}\,\alpha)$
10	Two-dimensional Avrami–Erofeev	A2: $2\,(1-\alpha)\,[-\ln(1-\alpha)]^{1/2}$
11	Three-dimensional Avrami–Erofeev	A3: $3\,(1-\alpha)\,[-\ln(1-\alpha)]^{2/3}$
12	*n*-Dimensional Avrami–Erofeev	A*n*: $\mathrm{n}\,(1-\alpha)\,[-\ln(1-\alpha)]^{1-1/\mathrm{n}}$
13	One-dimensional diffusion	D1: $1/(2\alpha)$
14	Two-dimensional diffusion	D2: $[-\ln(1-\alpha)]^{-1}$
15	Three-dimensional diffusion	D3: $1.5[1-(1-\alpha)^{1/3}]^{-1}\,(1-\alpha)^{2/3}$

J_kat is the catalytic constant; n is the reaction order; a is the catalytic index

where $\alpha_{exp,i}$ is the ith experimental conversion degree, $\alpha_{pre,i}$ is the *i*th predicted conversion degree, and N is the number of observations.

Results and discussion

Thermal decomposition behaviour

The isoperibolic experiment curves and data for the mixed solution at different ambient temperatures are shown in Fig. 2 and Table 2. A brown gas was observed in the mixed solution when the reaction temperature was at the maximum. For example, the temperature of the mixed system reached 367.45 K, which was 1.5 K higher than the ambient temperature. The results show that exothermic reactions occurred in the mixed acid solution when the reaction temperature was equal to 365.95 K, releasing a brown gas, i.e. NO_2, according to a study by Camera [11]. In addition, the time required to reach the maximum reaction temperature gradually decreased with increasing ambient temperature. This could be because the reaction rate increased with increasing ambient temperature.

The DSC curves for the nitric acid solution and the mixed solution obtained under different heating rates are shown in Figs. 3–5. The characteristic decomposition parameters are listed in Table 3. As shown in Fig. 3, in the high pressure crucible, thermal decomposition of the nitric acid solution started at 318.34 K. At this stage, the NO_2 gas produced might be directly dissolved in the nitric acid solution or liquefied into N_2O_4 before being dissolved in the solution. When the temperature approached the azeotropic point of the nitric acid solution (393.15 K for a 68.5% solution, according to Li [31]), part of the nitric acid solution was vapourized, and the maximum endothermic rate was attained at 398.71 K. Finally, the vapourization and liquefaction processes occurred at the same rate, resulting in a stable exothermic signal, as shown in Fig. 3. In the atmospheric pressure crucible (a crucible with a small hole), the solution first absorbed heat and was volatilized with a low rate constant. Then, the decomposition process started at 356.70 K with the evaporation of nitric acid, water, and NO_2, which resulted in the peak tail. The solution started boiling as the temperature approached the azeotropic point, 394.30 K. Afterwards, the gaseous nitric acid was pyrolysed in the crucible. Thus, there were two overlapping endothermic peaks instead of one peak, as shown in Fig. 3.

As shown in Fig. 4, in the temperature range from 303.15 to 351.24 K, the curve for the nitric acid solution is a horizontal line, while the curve for the mixed solution is a downward sloping line. This demonstrates that NPN was hydrolysed in the nitric acid solution. The *n*-propyl alcohol

Table 2 Isoperibolic experimental parameters for mixed solution including NPN and nitric acid solution at different ambient temperatures

T_0/K	T_{max}/K	t_{max}/s
340.15	341.45	254
344.85	346.15	200
349.95	351.55	175
354.65	356.45	152
359.55	361.15	138
365.95	367.45	118

T_0 is the ambient temperature; T_{max} is the maximum reaction temperature in the mixed system; t_{max} is the corresponding time

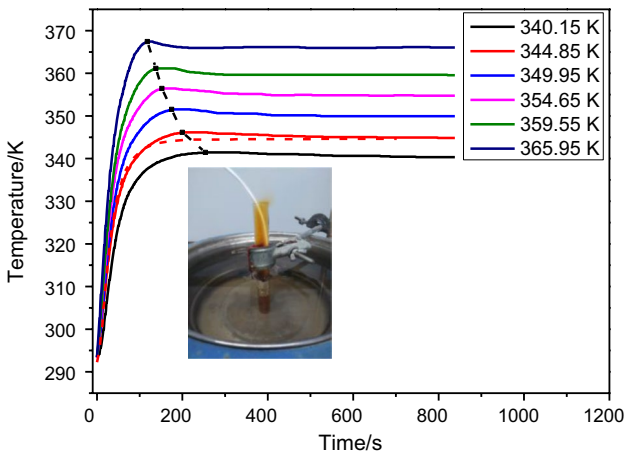

Fig. 2 Isoperibolic experiment curves for mixed solution including NPN and nitric acid solution at different ambient temperatures. (The red dashed line indicates isoperibolic experimental curve for nitric acid solution.)

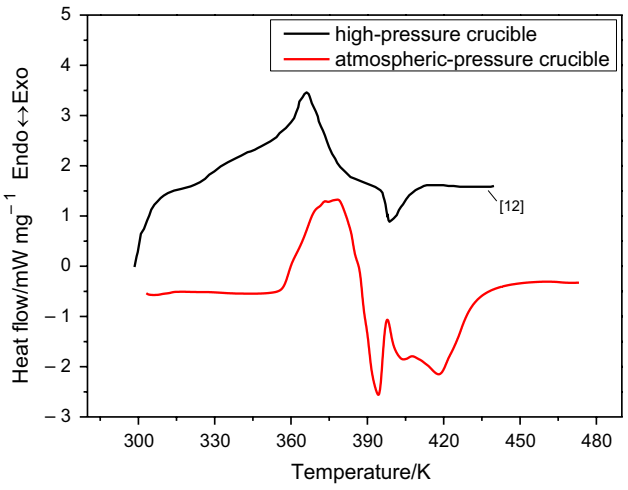

Fig. 3 DSC curves for nitric acid solution at 10 K min^{-1} in high pressure crucible and atmospheric pressure crucible. (The data in high pressure crucible were obtained from Ref. [12])

Table 3 Decomposition characteristics of all samples

Sample	β/K min^{-1}	First exothermic peak						
		T_i/K	T_e/K	T_{p1}/K	T_f/K	ΔH/J g^{-1}	T_{p2}/K	T_{p3}/K
1#[12]	10	–	318.34	365.42	393.53	311.09	398.71	–
2#	10	351.24	356.70	378.30	387.80	226.60	394.30	418.00
3#	8	349.28	351.70	376.20	386.80	152.70	397.60	–
4#	10	352.48	355.20	378.60	390.00	183.30	396.80	416.60
5#	12	356.35	358.80	379.70	392.70	294.80	–	416.00

1# nitric acid solution in high pressure crucible (obtained from Ref. [12]); 2# nitric acid solution in atmospheric pressure crucible; 3# mixed solution at 8 K min^{-1}; 4# mixed solution at 10 K min^{-1}; 5# mixed solution at 12 K min^{-1}. T_i is the initial temperature of exothermic peak; T_e is the onset temperature of exothermic peak; T_{p1} is the first exothermic peak temperature; T_f is the final temperature of exothermic peak; ΔH is the reaction heat of exothermic peak; T_{p2} is the first endothermic peak temperature; T_{p3} is the second endothermic peak temperature

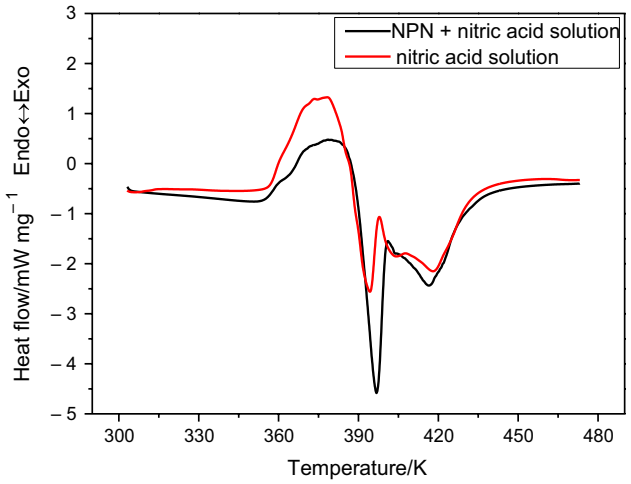

Fig. 4 DSC curves for nitric acid solution and mixed solution at 10 K min^{-1}

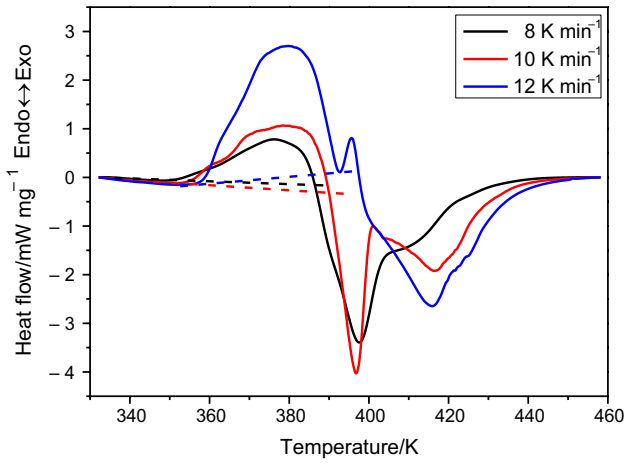

Fig. 5 DSC curves for the mixed solution with baselines at different heating rates: **a** 8 K min^{-1}; **b** 10 K min^{-1}; **c** 12 K min^{-1}

that was formed by this reaction was rapidly oxidized by the excess nitric acid, with an onset temperature of 355.20 K. This temperature is exactly within the thermolysis temperature range of the mixed solution, 340.15–365.95 K, as shown in Fig. 2. In addition, compared with the nitric acid solution, the onset temperature of the mixed solution decreased by 1.5 K, the maximum exothermic rate per unit decreased, and the heat of reaction decreased by 43.3 J g^{-1}. This might be because decomposition of the nitric acid solution is inhibited by oxidation. Then, the decomposition process was similar for both the mixed solution and the nitric acid solution.

From the above results, we can conclude that there is a difference between the pyrolysis process of a small amount of NPN in a nitric acid solution and a large amount of nitrate esters in a nitric acid solution. The former is an exothermic oxidation reaction that takes place with an excess of nitric acid solution after a hydrolysis process, while the latter is the pyrolysis of nitrate esters catalysed by the NO_2 produced from the decomposition of nitric acid [12]. In addition, the first exothermic peak derived from the DSC curves corresponded to the heating effect of the oxidation of NPN and the decomposition of nitric acid in the mixed solution. Therefore, the decomposition process of the mixed solution started with the hydrolysis of NPN, and the *n*-propyl alcohol that formed was then oxidized by nitric acid, in accordance with the study by Camera [11]. At this stage, the nitric acid was also decomposed. With increasing temperature, the reaction products, i.e. nitric acid and water, were volatilized, and the nitric acid vapour was pyrolysed.

Thermal decomposition kinetics

As shown in Fig. 5, the heat generated due to decomposition overlaps with the heat absorbed due to phase transition; this phenomenon is known as "a coupling phenomenon of heat generation and absorption", which is similar to "a coupling phenomenon of heat absorption and generation" [32].

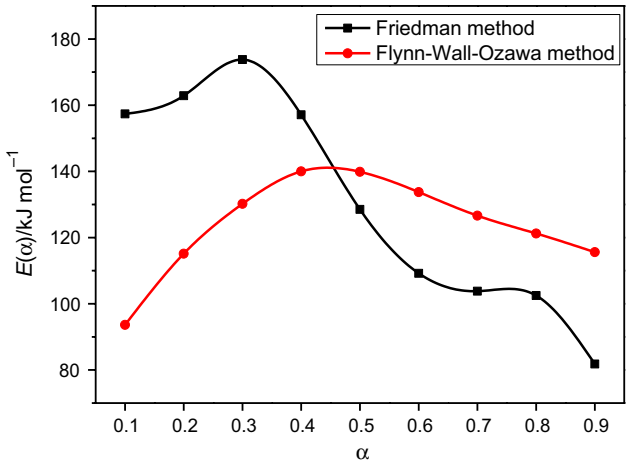

Fig. 6 Activation energy derived from the Friedman analysis and Flynn–Wall–Ozawa analysis for the decomposition of the mixed solution

Thus, the baselines were added in accordance with the recommendations reported in the literature [33, 34]. There is a significant overlap between the exothermic and endothermic peaks for a heating rate of 12 K min^{-1}, which demonstrates that the mixed solution reached its boiling point before the end of the decomposition process. The selected baseline is shown in Fig. 5.

The results from the Friedman and FWO analyses are shown in Fig. 6 for conversion degrees in the range of 0.1–0.9 and before the phase transition of the nitric acid solution. The activation energy values obtained using the FWO method range from 93.62 to 140.01 kJ mol^{-1}, with an average value of 124.01 kJ mol^{-1}, whereas those obtained using the Friedman method range from 81.79 to 173.79 kJ mol^{-1}, with an average value of 130.77 kJ mol^{-1}. As shown in Fig. 6, the average activation energy values determined by the two methods are approximately equal; however, the variation in the values acquired from the Friedman analysis is higher. Therefore, the average activation energy derived from the FWO analysis was selected as the decomposition activation energy. In addition, the activation energy derived from the two methods first increases and then decreases with increasing conversion degree from an overall perspective of Fig. 6. The activation energy represents the minimum energy requirement for a reaction to start; in other words, a higher activation energy means a slower reaction rate and a greater difficulty for starting a reaction. This could be because the propanol formed from the hydrolysis of NPN was easily and rapidly oxidized by nitric acid at small conversion degrees, and then, the concentration of propanol tapered off with increasing conversion degrees. Finally, the nitric acid was decomposed. According to the thermal decomposition behaviour of the mixed solution, the oxidation is easier than the pyrolysis of nitric acid.

Table 4 Statistics parameters obtained from different typical reaction kinetic models by nonlinear regression

Model no	Correlation coefficient	Least squares	Mean residual
1	0.996217	12.77804	0.02648
2	0.966164	112.57206	0.07538
3	0.998788	4.11455	0.01373
4	0.997551	8.29704	0.01904
5	0.998752	4.23581	0.01382
6	0.847832	475.13586	0.13980
7	0.999218	2.65151	0.01113
8	0.998922	3.65629	0.01343
9	0.998788	4.11575	0.01373
10	0.971620	94.54904	0.06565
11	0.934074	215.44918	0.09720
12	0.999196	2.72430	0.01119
13	0.971208	95.90628	1.95136
14	0.953985	151.92956	0.09370
15	0.929760	229.13247	0.11559

The reason is also why the activation energy for a small conversion degree is the lowest in the curve for the FWO analysis. These results also show that it is correct to select the average activation energy derived from the FWO analysis.

The results from a nonlinear regression analysis with 15 common kinetic models are summarized in Tables 4, 5, and Fig. 7. A comparison of the measured and calculated kinetic data is given in Fig. 8. According to Table 4 and Fig. 7, the best model is model No. 7, i.e. the *n*th Prout–Tompkins equation with autocatalysis [35], due to it having the maximum correlation coefficient (0.999218), the minimum LS (2.65151), and the minimum MR (0.01113). The most probable mechanism function of decomposition was found to be the 0.9082th Prout–Tompkins equation with autocatalysis, with a differential kinetic mechanism function of $f(\alpha)=(1-\alpha)^{0.9082}\cdot\alpha^{0.1291}$. In addition, the pre-exponential factor was equal to 2.754×10^{15} s^{-1}, and the activation energy was 124.01 kJ mol^{-1}. The decomposition kinetic model is expressed in Eq. (11):

$$\frac{d\alpha}{dt}=f(\alpha)A\exp(-E/RT)=2.754\times10^{15}\exp(-14915.80/T)(1-\alpha)^{0.9082}\alpha^{0.1291} \quad (11)$$

As shown in Table 6, compared with the two kinetic parameters calculated from the KAS and Kissinger methods, the relative deviations of the activation energy calculated with nonlinear regression are 0.05% and 2.18%, respectively. The relative deviations of the base-10 logarithm of the pre-exponential factor are 0.72% and 2.15%, respectively. Moreover, the values of these two kinetic parameters were both

Table 5 Most probable mechanism function and associated parameters derived from nonlinear regression analysis

Name	Differential function	lg$A$/s^{-1}	E/kJ mol^{-1}	n	a	Correlation coefficient
nth Prout–Tompkins equation with autocatalysis	$(1-\alpha)$^n* α^a	15.44	124.01	0.9082	0.1291	0.999218

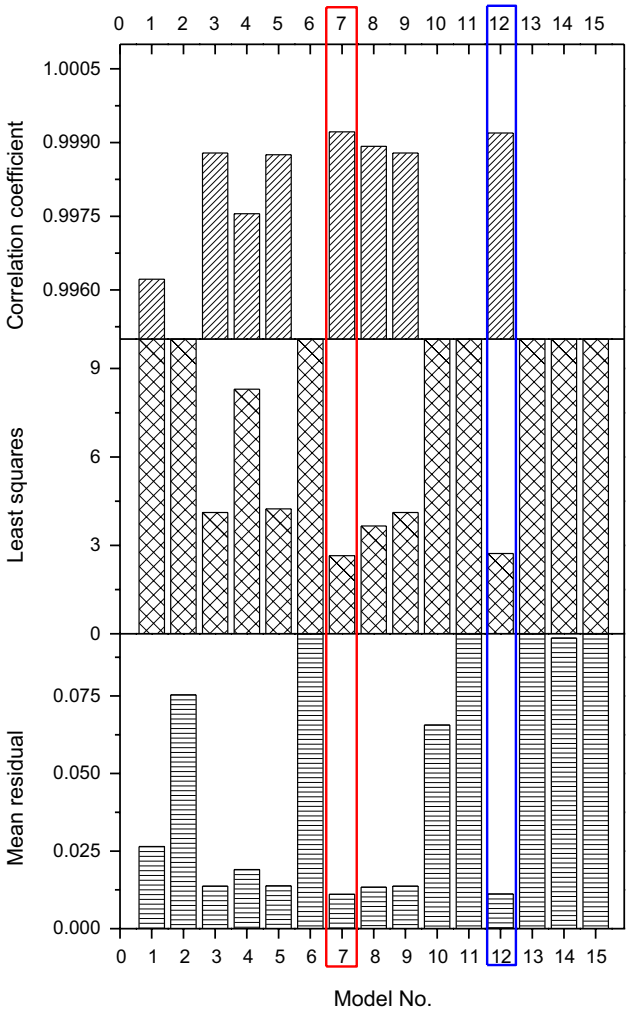

Fig. 7 Comparisons of evaluating parameters for different kinetic models collected. (The red box indicates the best model called "*n*th Prout–Tompkins equation with autocatalysis", and the blue box indicates the better model called "reaction of nth order with autocatalysis")

in the 95% CI. As Trache [27] stated, the results between the FWO and KAS methods are credible and accurate when these deviations are less than 5%. Thus, the results validated the accuracy and reliability of the kinetic parameters obtained from the FWO method and nonlinear regression.

According to Bohn [36], the thermal decomposition contains two parts: the first part is the intrinsic decomposition, and the second part is the autocatalytic decomposition. Therefore, the NO_2 formed played the role of a catalyst during the decomposition process, as reported in a study by

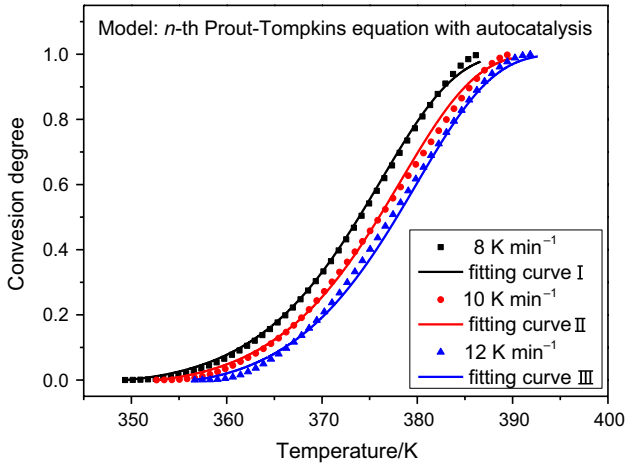

Fig. 8 Experimental and fitting curves derived from nonlinear regression analysis for the decomposition of the mixed solution

Camera [11]. In addition, the value of the activation energy was lower than that of some nitrate esters [37, 38], i.e. EHN and pentaerythritol tetranitrate (PETN), which indicates that the thermolysis of the mixed solution was easier than the pyrolysis of those nitrate esters. In other words, the heat sensitivity of the mixed solution was higher than that of the nitrate esters.

Thermodynamic properties

The critical temperature of thermal runaway (T_b) is a very important parameter for the mixed solution and was obtained by substituting E and T_{eo} (or T_{po}) into Eq. (12), according to the studies by Yan et al. [39–41].

$$T_b = \frac{E - \sqrt{E^2 - 4ERT_{eo/po}}}{2R} \tag{12}$$

where E is the activation energy /kJ mol^{-1} and $T_{eo/po}$ is the critical environment temperature /K, also known as the self-accelerating decomposition temperature (SADT). It is obtained by Eq. (13):

$$T_{e/p} = T_{eo/po} + b\beta_i + c\beta_i^2, \quad i = 1, 2, 3 \tag{13}$$

where T_e is the onset temperature /K, T_p is the peak temperature /K, b and c are the coefficients, and β_i is the heating rate of the sample /K min^{-1}.

Table 6 Some parameters to check kinetic parameters result with two model-free routes: KAS and Kissinger methods

Method	A	$G(\alpha)$	E/kJ mol^{-1}	lg$A$/s^{-1}	R	CI (95%)	
						E/kJ mol^{-1}	lg$A$/s^{-1}
KAS	0.10	0.14	93.40	10.69	0.99712	123.95 ± 9.11	15.33 ± 1.35
	0.20	0.29	114.80	13.98	0.99925		
	0.30	0.44	130.38	16.28	0.99919		
	0.40	0.61	140.02	17.67	0.99982		
	0.50	0.81	139.90	17.64	0.99535		
	0.60	1.03	133.71	16.76	0.98758		
	0.70	1.31	126.60	15.75	0.97872		
	0.80	1.67	121.06	14.97	0.97312		
	0.90	2.27	115.69	14.24	0.97456		
Kissinger	0.61	1.05	126.78	15.78	0.98676	126.78 ± 20.84	15.78 ± 6.30

CI (95%) is confidence interval under confidence level of 0.05

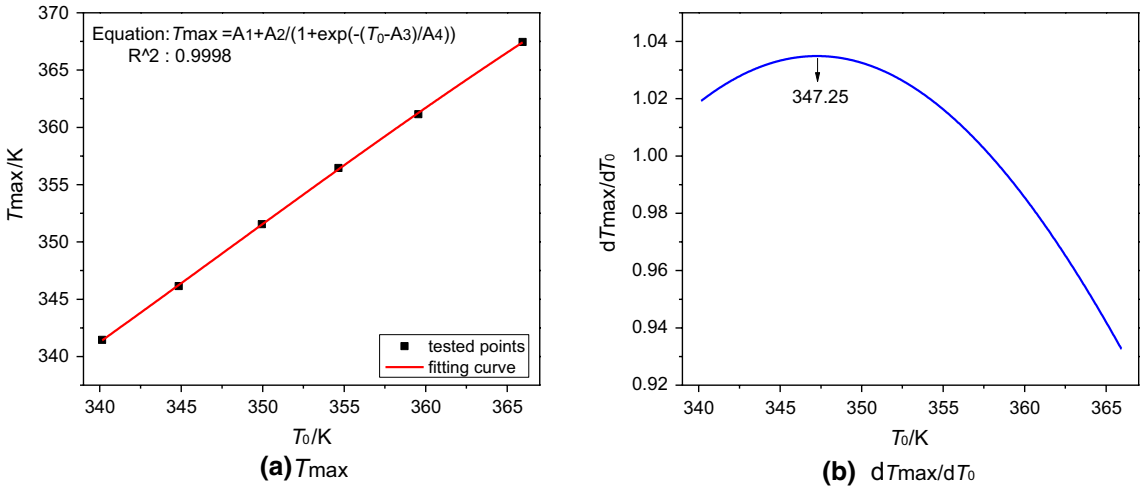

Fig. 9 Critical environment temperature obtained by Morbidelli and Varma criterion based on isoperibolic experiment data

The free energy of activation ($\Delta G^{\neq}$), enthalpy of activation ($\Delta H^{\neq}$), and entropy of activation ($\Delta S^{\neq}$) for the main exothermic decomposition reaction are obtained by Eqs. (14)–(16), listed in Table 6. In addition, T_{eo} is an important parameter when determining the thermodynamic properties, according to Zhang et al. [42].

$$A\exp\left(-\frac{E}{RT_{eo/po}}\right)=\frac{k_B T_{eo/po}}{h}\exp\left(-\frac{\Delta G^{\neq}}{RT_{eo/po}}\right) \tag{14}$$

$$\Delta H^{\neq}=E-RT_{eo/po} \tag{15}$$

$$\Delta G^{\neq}=\Delta H^{\neq}-T_{eo/po}\Delta S^{\neq} \tag{16}$$

Here k_B is the Boltzmann constant (1.3807×10^{-23} J K^{-1}) and h is the Planck constant (6.626×10^{-34} J K^{-1}).

Table 7 Thermodynamic parameters for the mixed solution based on isoperibolic and non-isothermal data

Thermodynamic parameters	Non-isotherm	Isoperibol	Avg
T_{eo}/K	338.70	347.25	–
T_b/K	346.76	355.73	–
$\Delta G^{\neq}$/kJ mol^{-1}	107.21	106.86	107.04
$\Delta H^{\neq}$/kJ mol^{-1}	121.19	121.12	121.16
$\Delta S^{\neq}$/J mol^{-1} K^{-1}	41.275	41.066	41.171

The critical environment temperature was obtained using the Morbidelli and Varma criterion [43, 44] and the isoperibolic experiment data, as shown in Fig. 9. The critical environment temperature was 347.25 K; compared with the values obtained from the onset temperature of the non-isothermal DSC data (Table 7), the critical environment temperature was 8.55 K higher. This may be because the heat

loss in an aluminium pan with a small hole is lower than that in a test tube. In addition, according to several previous reports [12, 45], the SADT of NPN is 383.15–392.15 K, and the onset temperature of nitric acid is 468.48 K based on the ARC results. These results show that the thermal stability of the mixed solution in an open system was higher than that in an approximately closed system. Second, the stability of the mixed solution was lower than that of NPN and nitric acid. In other words, spent acid was more hazardous than the NPN and nitric acid solution.

The free energies of activation, enthalpies of activation, and entropies of activation for the two systems during decomposition were approximately the same, as shown in Table 7. In addition, the positive value for the free energy indicates that the exothermic decomposition reaction of the mixed solution must proceed under heating conditions [46]. The activation enthalpy is similar to the activation energy, acting as an energy barrier required for reaction, and the activation entropy is used to measure the disorder in the system. Compared with those of *N*-2′,4′-dinitrophenyl-3,3-dinitroazetidine (DNPDNAZ, a good energetic material candidate) [39], the values of the free energy of activation and enthalpy of the mixed solution were lower, but the activation entropy was higher. This shows that the mixed solution system was more chaotic and decomposed more readily, in line with the results from contrasting the SADT and the critical temperature.

Conclusions

The following conclusions can be drawn:

(1) According to isoperibolic experiments and non-isothermal DSC, the decomposition in spent acid involves two competing reactions: the decomposition of NPN in a nitric acid solution and the decomposition of nitric acid. Specifically, the decomposition of the mixed solution starts with the hydrolysis of NPN, forming *n*-propyl alcohol, which is then oxidized by nitric acid. Additionally, the nitric acid is decomposed.

(2) Using an isoconversional method and nonlinear regression, we proved that the decomposition in the mixed solution follows a 0.9082th Prout–Tompkins equation with autocatalysis, with a differential kinetic mechanism function of $f(\alpha)=(1-\alpha)^{0.9082}\cdot\alpha^{0.1291}$. Moreover, the activation energy and pre-exponential factor were 124.01 kJ mol^{-1} and 2.754×10^{15} s^{-1}, respectively.

(3) The critical environment temperatures (or SADT) of the mixed solution, obtained from isoperibolic and non-isothermal data, were 347.25 K and 338.70 K. The critical temperatures of thermal runaway were 355.73 K and 346.76 K, indicating that the thermal stability of the mixed solution in an open system was higher than that of the mixed solution in an approximately closed system. Second, the spent acid was more hazardous than NPN (SADT = 383.15–392.15 K) and nitric acid (T_{oneset} = 468.48 K). The free energies of activation, enthalpies of activation, and entropies of activation were the same for the isoperibolic experiments and non-isothermal DSC, with average values of 107.04 k J mol^{-1}, 121.16 k J mol^{-1}, and 41.171 J mol^{-1} K^{-1}, respectively.

References

1. Rigas F, Sebos I, Doulia D. Safe handling of spent acids in nitroglycerine/nitroglycol plants. J Loss Prevent Proc. 1998;11:161–8.
2. Chen CY, Wu CW, Duh YS, et al. An experimental study of worst case scenarios of nitric acid decomposition in a toluene nitration process. Process Saf Environ. 1998;76:211–6.
3. Lu KT, Lin PC. Study on the stability of nitroglycerine spent acid. Process Saf Environ. 2009;87:87–93.
4. Larkin A, Geddes JA, Martin RV, et al. global land use regression model for nitrogen dioxide air pollution. Environ Sci Technol. 2017;51:6957–64.
5. Levy JB, Adrian FJ. The thermal decomposition of nitrate esters. III. *n*-propyl nitrate. J Am Chem Soc. 1955;77:2015–6.
6. Hiskey MA, Brower KR, Oxley JC. Thermal decomposition of nitrate esters. J Phys Chem. 1991;95:3955–60.
7. Zeng XL, Chen WH, Liu JC, et al. A theoretical study of five nitrates: electronic structure and bond dissociation energies. J Mol Struc-Theochem. 2007;810:47–51.
8. Zeng XL, Chen WH, Liu JC, et al. Experimental and theoretical studying the thermolysis of nitrate. J Therm Anal Calorim. 2008;91:359–63.
9. Wang J, Liu DB, Zhou XL. Studies on the thermal decomposition kinetic of a nitrate Ester. Appl Mech Mater. 2012;182:1575–80.
10. Camera E, Modena G, Zotti B. On the behaviour of nitrate esters in acid solution. II. Hydrolysis and oxidation of nitroglycol and nitroglycerin. Propell Explos Pyrot. 1982;7:66–9.
11. Camera E, Modena G, Zotti B. On the behaviour of nitrate esters in acid solution. III. Oxidation of ethanol by nitric acid in sulphuric acid. Propell Explos Pyrot. 1983;8:70–3.
12. Yang T, Chen L, Chen W, et al. Thermal stability of 2-ethylhexyl nitrate with acid. J Therm Anal Calorim. 2015;119:205–12.
13. Pourmortazavi SM, Rahimi-Nasrabadi M, Kohsari I, et al. Non-isothermal kinetic studies on thermal decomposition of energetic materials. J Therm Anal Calorim. 2012;110:857–63.
14. Pourmortazavi SM, Farhadi K, Mirzajani V, et al. Study on the catalytic effect of diaminoglyoxime on thermal behaviors, non-isothermal reaction kinetics and burning rate of homogeneous double-base propellant. J Therm Anal Calorim. 2016;125:121–8.
15. Abusaidi H, Ghaieni HR, Pourmortazavi SM, et al. Effect of nitro content on thermal stability and decomposition kinetics of nitro-HTPB. J Therm Anal Calorim. 2016;124:935–41.
16. Pourmortazavi SM, Rahimi-Nasrabadi M, Rai H, et al. Role of metal oxide nanomaterials on thermal stability of 1,3,6-trinitrocarbazole. Propell Explos Pyrot. 2016; 41.
17. Pourmortazavi SM, Rahimi-Nasrabadi M, Rai H, et al. Effect of nanomaterials on thermal stability of 1,3,6,8-tetranitro carbazole. Cent Eur J Energ Mat. 2017;14:201–16.

18. Pourmortazavi SM, Kohsari I, Zandavar H, et al. Electrospinning and thermal characterization of nitrocellulose nanofibers containing a composite of diaminofurazan, aluminum nano-powder and iron oxide nanoparticles. Cellulose. 2019;26:4405–15.
19. Pourmortazavi SM, Mirzajani V, Farhadi K. Thermal behavior and thermokinetic of double-base propellant catalyzed with magnesium oxide nanoparticles. J Therm Anal Calorim. 2019;137:93–104.
20. Friedman HL. Kinetics of thermal degradation of char-forming plastics from thermogravimetry. Application to a phenolic plastic. J Polym Sci Pol Lett. 1964;6:183–95.
21. Venkatesh M, Ravi P, Tewari SP. Isoconversional kinetic analysis of decomposition of nitroimidazoles: Friedman method versus Flynn-Wall-Ozawa method. J Phys Chem A. 2013;117:10162–9.
22. Ozawa T. A new method of analyzing thermogravimetric data. Bull Chem Soc Jpn. 1965;38:1881–6.
23. Flynn JH, Wall LA. A quick, direct method for the determination of activation energy from thermogravimetric data. J Poly Sci B Poly Lett. 1966;4:323–8.
24. Kissinger HE. Reaction kinetics in differential thermal analysis. Anal Chem. 1957;29:1702–6.
25. Juibari NM, Eslami A. Investigation of catalytic activity of $ZnAl_2O_4$ and $ZnMn_2O_4$ nanoparticles in the thermal decomposition of ammonium perchlorate. J Therm Anal Calorim. 2017;128:115–24.
26. Söyleyici S, Çılgı GK. Thermal and kinetic analyses of 2,5-bis(2-hydroxyphenyl)- thiazolo[5,4-d]thiazole. J Therm Anal Calorim. 2014;118:705–9.
27. Trache D, Maggi F, Palmucci I, et al. Thermal behavior and decomposition kinetics of composite solid propellants in the presence of amide burning rate suppressants. J Therm Anal Calorim. 2018;132:1601–15.
28. Bruijn TJWD, Jong WAD, Berg PJVD. Kinetic parameters in Avrami-Erofeev type reactions from isothermal and non-isothermal experiments. Thermochim Acta. 1981;45:315–25.
29. Pielichowska K. The influence of polyoxymethylene molar mass on the oxidative thermal degradation of its nanocomposites with hydroxyapatite. J Therm Anal Calorim. 2016;124:751–65.
30. Zhang YX, Chen HH, Chen T. Drying kinetics of RDX under atmospheric pressure and vacuum conditions. Energy Convers Manage. 2014;80:266–75.
31. Li HC, Fu B. Handbook of practical chemistry. Bei Jing: Chemical Industry Press; 2007.
32. Zhang CX, Lu GB, Chen LP, et al. Two decoupling methods for non-isothermal DSC results of AIBN decomposition. J Hazard Mater. 2015;285:61–8.
33. Riesen R. Choosing the right baseline. User Commun. 2007;25:1–6.
34. Kučerík J, Schwarz J, Jäger A, et al. Character of transitions causing the physicochemical aging of a sapric histosol. J Therm Anal Calorim. 2014;118:1169–82.
35. Burnham AK. Application of the Šesták-Berggren Equation to Organic and Inorganic Materials of Practical Interest. J Therm Anal Calorim. 2000;60:895–908.
36. Bohn MA. Problems and faulty uses with the Prout-Tompkins description of autocatalytic reactions and the solutions. J Therm Anal Calorim. 2014;116:1–12.
37. Yan QL, Künzel M, Zeman S, et al. The effect of molecular structure on thermal stability, decomposition kinetics and reaction models of nitric esters. Thermochim Acta. 2013;566:137–48.
38. Lu G, Yang T, Chen L, et al. Thermal decomposition kinetics of 2-ethylhexyl nitrate under non-isothermal and isothermal conditions. J Therm Anal Calorim. 2016;124:471–8.
39. Yan B, Li HY, Zhao NN, et al. Thermodynamic properties, detonation characterization and free radical of *N*-2′,4′-dinitrophenyl-3,3-dinitroazetidine. J Chem Thermodyn. 2014;69:152–6.
40. Li HY, Yan B, Guan YL, et al. Thermodynamic properties, detonation characterisation and free radical of *N*-acetyl-3,3-dinitroazetidine. J Chem Thermodyn. 2015;90:87–91.
41. Yan B, Li HY, Guan YL, et al. Thermodynamic properties of 3,3-dinitroazetidinium nitrate. J Chem Thermodyn. 2016;103:206–11.
42. Zhang T, Hu R, Xie Y, et al. The estimation of critical temperatures of thermal explosion for energetic materials using non-isothermal DSC. Thermochim Acta. 1994;244:171–6.
43. Morbidelli M, Varma A. A generalized criterion for parametric sensitivity: application to thermal explosion theory. Chem Eng Sci. 1988;43:91–102.
44. Broccanello A. Prediction criteria of thermal runaway in the acid catalyzed esterification of acetic anhydride. Univ. of Padova. 2016.
45. Yang Q, Chen LP, Chen WH, et al. Research on the thermal stability of four nitrates by accelerating the rate calorimeter. J Saf Environ. 2012;1:188–92.
46. Wang P, Xie Q, Xu Y, et al. A kinetic investigation of thermal decomposition of 1,1′-dihydroxy-5,5′-bitetrazole-based metal salts. J Therm Anal Calorim. 2017;130:1213–20.

Publisher's Note Springer Nature remains neutral with regard to jurisdictional claims in published maps and institutional affiliations.